Magnetic dipolarizations inside geosynchronous orbit with tailward ions flow

Xiaoying Sun[1,2], Weining William Liu [1], Suping Duan[1]

[1] State Key Laboratory of Space Weather, National Space Science Center (NSSC),Chinese Academy of Sciences (CAS), Beijing, 100190, China

[2]University of Chinese Academy of Sciences, Beijing, 100049, China

Correspondence to: W .W. Liu (wliu@nssc.ac.cn), Suping Duan (spduan@nssc.ac.cn)

Abstract. Electromagnetic field and plasma data from the Time History of Events and Macroscale Interactions during Substorms (THEMIS) near-Earth probes are used to investigate magnetic dipolarizations inside geosynchronous orbit on 27 August 2014 during an intense substorm with AE_{max} ~ 1000nT. THEMIS-D (TH-D) was located inside geosynchronous orbit around midnight in the interval from 09:25 UT to 09:55 UT. During this period two distinct magnetic dipolarizations with tailward ions flow are observed by TH-D. The first one is displayed by magnetic elevation angle increase from 15 degree to 25 degree around 09:30:40UT. The tailward perpendicular velocity is $V_{\perp \mathrm{x}}$ ~ -50km/s. The second one is presented by the elevation angle increase from 25 degree to 45 degree around 09:36 UT. And the tailward perpendicular velocity is $V_{\perp \mathrm{x}}$ ~ -70 km/s. These two significant dipolarizations are accompanied with the sharp increase in the energy flux of energetic electron inside geosynchronous. After 5 min expanding of near-Earth plasma sheet (NEPS), THEMIS-E (TH-E) located outside geosynchronous orbit also detects this tailward expanding plasma sheet with ion flow -150 km/s. The dipolarization propagates tailward with speed -47 km/s, along 2.2 R_E distance in the X direction between TH-D and TH-E within 5 min. These dipolarizations with tailward ions flow observed inside geosynchronous orbit indicate new energy transfer path in the inner magnetosphere during substorms.

Keywords: Magnetic dipolarization, tailward ions flow, near-Earth plasma sheet, intense substorm

Introduction

Magnetic dipolarization can be observed at or inside geosynchronous orbit during intense substorms with high AE index ($AE > 500$ nT) [e.g., Dai et al., 2015; Nagai, 1982; Noséet al., 2014; Ohtani et al., 2018]. Dipolarizations are marked by the magnetic elevation angle increase with the decrease in the radial components of B_x and B_y, and the increase in the B_z component [Liu and Liang, 2009; Duan et al., 2011; Dai et al., 2014, 2015]. Ohtani et al. [2018] presented the statistics characteristics of magnetic dipolarizations inside geosynchronous orbit. They reported that the dipolarization region expanded in the azimuthal direction with speed 60 km/s at 5.5 R_E. Using multiple satellites conjunction observations at or

29 inside geosynchronous orbit, Dai et al. [2015] reported that the large dipolarization electric field was associated with
30 substorm injection of MeV electrons into the inner magnetosphere (r < 6.6 R_E).

31

32 Magnetic dipolarizations are accompanied with complex ions bulk flow in the near-Earth plasma sheet (NEPS) [e.g., Duan et
33 al., 2008; Liang et al., 2009]. Especially, it is more complex in the inner edge of NEPS. Usually, the substorm-associated
34 dipolarizations in the NEPS are accompanied with earthward ions bulk flow [e.g., Angelopoulos et al., 1992; Baumjohann et
35 al., 1999; Duan et al., 2011; Liang et al., 2009; Liu et al., 2008; Nakamura et al., 2009; Shiokawa et al., 1998]. According
36 conjunction observations of THEMIS multiple probes in the NEPS, Duan et al. [2011] pointed out that the dipolarization at
37 inner edge of the near-Earth plasma sheet had no one-to-one relationship with the earthward ions bulk flow. Lui et al. [1999]
38 pointed out that dipolarization at $X \sim 10\,R_E$ was detected with tailward flow. Inside geosynchronous orbit, magnetic
39 dipolarizations were detected with earthward ions bulk flow [Dai et al., 2015].

40

41 Near-Earth Dipolarizations with low frequency waves are detected with thermal ions and electron energization [e.g., Dai et
42 al., 2015; Liang et al., 2009; Nosé et al., 2014; Ohtani et al., 2018]. These energetic particles are main source of inner
43 magnetosphere during substorms and storms. Nosé et al. [2014] proposed that the dipolarizations associated with low
44 frequency fluctuations were observed in the inner magnetosphere during the storm main phase. These low frequency
45 electromagnetic waves can accelerate O^+ ions in the perpendicular direction. The low frequency waves can accelerate
46 particles crossing the magnetic field with large perpendicular electric field [e.g., Dai et al., 2014, 2015; Duan et al., 2016;
47 Nosé et al., 2014]. Usually, Dipolarization associated dispersionless energetic particle injections is accompanied with
48 earthward ions bulk flow in the NEPS [Dai et al., 2015]. But few reports show that dipolarizations with the sharply increase
49 in the energy flux of energetic particles associated with tailward ions flow at or inside geosynchronous orbit.

50

51 The ballooning mode occurred in the near-Earth plasma sheet are associated with tailward expansion of plasma sheet during
52 substorms [Liu, 1997; Liu et al., 2008; Liu and Liang, 2009; Liang et al., 2009; Saito et al., 2008]. Liu et al. [2008] pointed
53 out that the ballooning mode could excite a quasi-electrostatic field a few minutes before local current disruption and that the
54 perturbations associated with ballooning instability propagated downtail.

55

56 In this paper we present dipolarizations with tailward ions flow inside geosynchronous orbit during an intense substorm
57 expansion phase. The observations in detail of an intense substorm on 27 August 2014 by TH-D and TH-E are presented in
58 section 2. Discussions and conclusions of our observation results are displayed in the last section.

59 **Observations of an intense substorm on 27 August 2014**

60 The OMNI data of the solar wind, interplanetary magnetic field (IMF) and geomagnetic field index Dst and AE during a

61 storm on August 27, 2014 are presented in Figure 1. The minimum value of $SYM - H$ index is about -90 nT, as shown in

62 Figure 1f, imply that a moderate storm take placed. During the main phase of this moderate storm, there is an intense

63 substorm with the AE maximum value 700 nT around 10:10 UT. The beginning time of this intense substorm expansion

64 phase is around 09:31 UT with decrease in the AL index. A significant substorm enhancement occur around 09:48 UT with

65 sharply decrease in the AL index and increase in the AE index.

66

67 During this intense substorm, THEMIS probes [Angelopoulos, 2008], such as TH-D and TH-E are both located in the near-

68 Earth magnetotail. Figure 2 displays the orbits of TH-D and TH-E from 09:20 to 10:00 UT in the SM coordinate system. At

69 09:30 UT, locations of these two spacecraft in SM coordinates, are (-6.10, -0.06, 0.43) R_E for TH-D, (-8.26, -2.28, 0.99) R_E

70 for TH-E, respectively. TH-D orbit plot presents that it is located inside geosynchronous orbit at the beginning time of this

71 intense substorm expansion phase. On the other hand, TH-E is located outside geosynchronous orbit. These two spacecraft

72 present good conjunction observations during this intense substorm expansion phase. The instruments adopted in our

73 investigations are the fluxgate magnetometer (FGM) [Auster et al., 2008], the electrostatic analyzer (ESA) [McFadden et al.,

74 2008], the electric field instrument (EFI) [Bonnell et al., 2008] and the solid state telescope (SST) on board the THEMIS

75 probes.

76

77 Figure 3 shows the plasma parameters and the electromagnetic field detected by TH-D mostly inside geosynchronous orbit at

78 about midnight section. The solar magnetic (SM) coordinate system is adopted. From top to bottom, panels are the total

79 magnetic field value, B_t and the B_x component, the B_y and B_z components, the magnetic field elevation angle defined by

80 $\theta = \tan^{-1}(B_z/(B_x^2 + B_y^2)^{1/2})$, the ion and electron density, temperature, the plasma beta value β, $\beta = 2\mu_0 nT/B^2$, which

81 determines the location of the satellite [Miyashita et al., 2000], three components of ions bulk flow velocity parallel (black

82 line) and perpendicular (red line) to the magnetic field, V_x, V_y and V_z, three components of the electric field, the E_x (red), the

83 E_y (black) and the E_z (blue), there components of convection electric field from $\mathbf{V} \times \mathbf{B}$, the E_{cx} (red), the E_{cy} (black) and the

84 E_{cz} (blue), respectively. Figure 3 displays the distinct fluctuations of the magnetic field and plasma density and velocity

85 around 09:30 UT and 09:36 UT, respectively. The magnetic elevation angle has two step clear enhancements as displayed in

86 Figure 3c. The first increase in elevation angle is from about 15 degree to 25 degree during the interval from 09:30:34 UT to

87 09:30:54 UT, which are marked by the left two vertical dashed lines in Figure 3. The total magnetic field value and the B_x

88 component both decrease. The B_z component increase weakly from about 35 nT to 45 nT. The B_y component has obvious

89 fluctuations around 0 nT. These magnetic signatures indicate a magnetic dipolarization take places inside geosynchronous

90 orbit around (-6.10, -0.06, 0.43) R_E. During this weak magnetic field dipolarization, the plasma beta value, β, increases from

91 around 0.5 to 1.0. The electron density and temperature both increase. The ion density also increases. But ion temperature

92 decreases. Accompanied this dipolarization the tailward ions bulk flow, $V_{//x}$ ~ -100km/s and the perpendicular component

93 to the magnetic field in the X direction, $V_{\perp x}$ ~ -50 km/s is detected by TH-D, as shown in Figure 3g. The perpendicular

94 velocity in the Y direction is mainly dawnward at the beginning time of this dipolarization, $V_{\perp y}$ ~ -30km/s. The electric

95 field detected by TH-D also has large fluctuations with negative E_y value during the first depolarization as shown in Figure

96 3j. During the intervals from 09:30:34 UT to 09:30:54 UT the convection electric field direction is dawnward with large

97 magnitude, E_{cy} ~ -12 mV/m, as presented in Figure 3k. The second magnetic field elevation angle increases sharply at

98 around 09:36 as displayed in Figure 3c marked by the right two vertical dashed lines. The elevation angle increases from

99 about 25 degree to 45 degree during the interval from 09:36:06 UT to 09:36:21UT. The magnetic field has similar variations

100 to the first dipolarization signatures. Especially, the second dipolarization has larger elevation angle maximum value, ~ 45

101 degree, as marked by the fourth vertical dashed line in Figure 3c. During the second dipolarization the tailward ions bulk

102 flow perpendicular to the magnetic field is also detected by TH-D, $V_{\perp x}$ ~ -70 km/s, as presented in Figure 3g. Also the

103 significant negative E_y component is companied by this intense dipolarization in Figure 3j and 3k.

104

105 During the intervals of magnetic dipolarizations with tailward ions bulk flow detected by TH-D inside geosynchronous orbit,

106 TH-E observed very weak increase in the magnetic field elevation angle and the B_z component around 09:35 UT and 09:41

107 UT, as shown in Figure 4b and 4c, about 5 min after two dipolarizations detected by TH-D. The ions and electron density

108 and temperature increase weakly from very low value as displayed in Figure 4d and 4e. Outside geosynchronous orbit, TH-E

109 observed very low beta value, as shown in Figure 4f, β ~ 0.01 and β ~ 0.2 around 09:35 UT and 09:41 UT, respectively.

110 Interesting phenomena that the weak dipolarization was with the tailward ions bulk flow, $V_{//x}$ ~ -180km/s, is also detected

111 by TH-E around 09:35 UT as shown in Figure 4g. The perpendicular velocity is dominated in the negative Y direction, $V_{\perp y}$ ~

112 -50 km/s.

113

114 Associated with the intense electric field observed by TH-D inside geosynchronous orbit during this two dipolarizations, the

115 energy fluxes of energetic electrons, as shown in the second panel of Figure 5, with energy of 31 keV(blue), 41 keV(gray),

116 52 keV (red), 65.5 keV (black), 93 keV(brown) and 139 keV(purple) all simultaneously increase at 09:30:38 UT and

117 09:36:09UT detected by SST/TH-D, respectively. These energetic electrons have quasi-perpendicular pitch angle

118 distribution, as presented in the bottom panel of Figure 5.

119 **Discussion and conclusions**

120 The dipolarizations with tailward ions bulk flow inside geosynchronous orbit are investigated in our present paper.

121 Accompanied these dipolarizations the energy fluxes of energetic electrons with energy between 31 keV and 139 keV

122 simultaneously increase inside geosynchronous orbit. According to these energetic electrons pitch angle distributions, it is

123   found that high energy electrons mainly in the quasi-perpendicular direction to the magnetic field, as shown in Figure 5. On

124   the other hand, the inductive electric field during these two magnetic dipolarization is in the dawnward direction as display

125   in Figure 3j and 3k. Previous research work reported that the inductive electric field associated with substorm dipolarization

126   can accelerate particles in the near-Earth plasma sheet [e.g. Dai et al., 2014, 2015; Duan et al., 2016; Fu et al., 2011; Fok et

127   al., 2001; Liu et al., 2010; Lui et al., 1988, 1999; Nakamura et al., 2009; Nos é et al., 2014]. As shown in Figure 3j around

128   09:36:30 UT the inductive electric fields in the second dipolarization are dominated in the E_y component with large negative

129   value, $E_y \sim$ -25mV/m, and the X component also increase with negative value $E_x \sim$ -6mV/m. This intense electric field can

130   drive ions moving into the tailward-dawnward direction. On the other hand, we can calculate the energy quantity relationship

131   between the electric field and energetic electrons. Estimating the energy of such intense E_y in the distance of ~1000 km is

132   about ~ 10^{-15} Joule. The energetic electrons with energy range from 31 keV to 139 keV are in the same energy order ~10^{-15}

133   Joule. It is inferred that the intense E_y can perpendicularly accelerate electrons to tens keV state.

134

135   Dipolarizations occurring at the inner edge of plasma sheet are complicated with disturbances of ions bulk flow and

136   electromagnetic field. Lui et al. [1999] pointed out that near-Earth dipolarization was a non-MHD process and was also

137   accompanied with tailward ions flow. Our observations of dipolarizations inside geosynchronous orbit are also associated

138   with tailward ions flow. This result is consistent with the report proposed by Liu et al. [2008] that the perturbations

139   associated with the ballooning mode in the near-Earth plasma sheet propagating tailward. Based on the statistic studies, Nos é

140   et al. [2016] proposed that the occurrence probability of the dipolarizations in the inner magnetosphere had a peak at 21:00-

141   00:00 MLT. Our observations show that two distinct dipolarizations with tailward flow inside geosynchronous orbit are

142   detected by TH-D around 00:02 MLT and 00:05 MLT, respectively.

143

144   According to the distance between TH-D and TH-E, (-2.23, -2.30, 0.56)R_E, and the delay time of dipolarization from inside

145   to outside geosynchronous orbit, ~5 min, the dipolarization propagating speed or the plasma sheet expanding speed can be

146   estimated as $V_x \sim$ -47 km/s, $V_y \sim$ -48 km/s, $V_z \sim$ 12 km/s, respectively. Liou et al. [2002] proposed that the dipolarization

147   region expanding speed was ~ 60 km/s westward at geosynchronous. Comparing observations between TH-D and TH-E in

148   our investigations, the azimuth speed of dipolarization region is obtained ~ 48 km/s. These two observational results are

149   consistent with each other. The dipolarization associated with the current disruption propagated tailward with speed $V_x \sim$ -

150   100 km/s detected by THEMIS satellites in the near-Earth plasma sheet X~ -11 R_E [Liu et al., 2008]. It is larger than the

151   dipolarization propagating speed from inside to outside geosynchronous orbit $V_x \sim$ -47 km/s . The different speeds of

152   dipolarizations propagating tailward imply that the magnitude of the dipolarization speed may be associated with its

153   beginning location in magnetotail plasma sheet.

154

155   On the other hand, Lui [1991] reported that substorm disturbance propagated tailward through a rarefaction wave front

156   accompanied by earthward flow during substorm expansion phase early period. Chao et al. [1977] proposed that the

157   rarefaction wave propagating tailward was accompanied by the thinning of plasma sheet and earthward plasma flow. This

158   earthward flow is possibly convection flow or outflow flow of magnetic reconnection from the middle magnetotail.

159

160   Based on the above observation analysis, we can draw the results as following. Two distinct magnetic dipolarizations with

161   tailward ions flow are observed by TH-D inside geosynchronous orbit on 27 August 2014 during the intense substorm with

162   AE_{max} ~ 1000nT. TH-D was located inside geosynchronous orbit around midnight in the interval from 09:20 UT to 10:00

163   UT. The first dipolarization is displayed by magnetic elevation angle increase from 15 degree to 25 degree around

164   09:30:40UT. The second one is presented by the elevation angle increase from 25 degree to 45 degree around 09:36 UT.

165   These two significant dipolarizations are accompanied with the energy flux of energetic electrons simultaneously increase

166   inside geosynchronous orbit. After 5 min expanding tailward of near-Earth plasma sheet, TH-E located outside

167   geosynchronous orbit also detects this tailward expanding plasma sheet with ion flow -150 km/s. The dipolarization

168   propagates tailward with speed -45 km/s, along 2 R_E distant in the X direction between TH-D and TH-E within 5 min.

169   These dipolarizations with tailward ion flow observed inside geosynchronous orbit indicate new energy transfer path in the

170   inner magnetosphere during substorms.

181   **References**

182   Angelopoulos, V.: The THEMIS Mission, Space Science Reviews, 141, 5-34, 2008.

183   Angelopoulos, V., Baumjohann, W., Kennel, C. F., Coroniti, F. V., Kivelson, M. G., Pellat, R., Walker, R. J., Lühr, H., and

184   Paschmann, G.: Bursty bulk flows in the inner central plasma sheet, Journal of Geophysical Research, 97, 4027, 1992.

185 Auster, H. U., Glassmeier, K. H., Magnes, W., Aydogar, O., Baumjohann, W., Constantinescu, D., Fischer, D., Fornacon, K.

186 H., Georgescu, E., Harvey, P., Hillenmaier, O., Kroth, R., Ludlam, M., Narita, Y., Nakamura, R., Okrafka, K., Plaschke, F.,

187 Richter, I., Schwarzl, H., Stoll, B., Valavanoglou, A., and Wiedemann, M.: The THEMIS Fluxgate Magnetometer, Space

188 Science Reviews, 141, 235-264, 2008.

189 Baumjohann, W., Hesse, M., Kokubun, S., Mukai, T., Nagai, T., and Petrukovich, A. A.: Substorm dipolarization and

190 recovery, Journal of Geophysical Research: Space Physics, 104, 24995-25000, 1999.

191 Bonnell, J. W., Mozer, F. S., Delory, G. T., Hull, A. J., Ergun, R. E., Cully, C. M., Angelopoulos, V., and Harvey, P. R.: The

192 Electric Field Instrument (EFI) for THEMIS, Space Science Reviews, 141, 303-341, 2008.

193 Chao J., K ., J. R . Kan, A . T. Y. Lui and S .-I. Akasofu A model for thinning of the plasma sheet, Planet. Space Sci., 25,

194 703-710, 1977.

195 Dai, L., Wang, C., Duan, S., He, Z., Wygant, J. R., Cattell, C. A., Tao, X., Su, Z., Kletzing, C., Baker, D. N., Li, X.,

196 Malaspina, D., Blake, J. B., Fennell, J., Claudepierre, S., Turner, D. L., Reeves, G. D., Funsten, H. O., Spence, H. E.,

197 Angelopoulos, V., Fruehauff, D., Chen, L., Thaller, S., Breneman, A., and Tang, X.: Near-Earth injection of MeV electrons

198 associated with intense dipolarization electric fields: Van Allen Probes observations, Geophys Res Lett, 42, 6170-6179, 2015.

199 Dai, L., Wygant, J. R., Cattell, C. A., Thaller, S., Kersten, K., Breneman, A., Tang, X., Friedel, R. H., Claudepierre, S. G.,

200 and Tao, X.: Evidence for injection of relativistic electrons into the Earth's outer radiation belt via intense substorm electric

201 fields, Geophysical Research Letters, 41, 1133-1141, 2014.

202 Duan, S., Liu, Z., Cao, J., Lu, L., R ème, H., Dandouras, I., and Carr, C. M.: TC-1 observation of ion high-speed flow

203 reversal in the near-Earth plasma sheet during substorm, Science in China Series E: Technological Sciences, 51, 1721-1730,

204 2008.

205 Duan, S. P., Dai, L., Wang, C., Liang, J., Lui, A. T. Y., Chen, L. J., He, Z. H., Zhang, Y. C., and Angelopoulos, V.: Evidence

206 of kinetic Alfven eigenmode in the near-Earth magnetotail during substorm expansion phase, Journal of Geophysical

207 Research-Space Physics, 121, 4316-4330, 2016.

208 Duan, S. P., Liu, Z. X., Liang, J., Zhang, Y. C., and Chen, T.: Multiple magnetic dipolarizations observed by THEMIS

209 during a substorm, Annales Geophysicae, 29, 331-339, 2011.

210 Fok, M.-C., Moore, T. E., and Spjeldvik, W. N.: Rapid enhancement of radiation belt electron fluxes due to substorm

211 dipolarization of the geomagnetic field, Journal of Geophysical Research: Space Physics, 106, 3873-3881, 2001.

212 Fu, H. S., Khotyaintsev, Y. V., André, M., and Vaivads, A.: Fermi and betatron acceleration of suprathermal electrons

213 behind dipolarization fronts, Geophysical Research Letters, 38, n/a-n/a, 2011.

214 Liang, J., Liu, W. W., and Donovan, E. F.: Ion temperature drop and quasi-electrostatic electric field at the current sheet

215 boundary minutes prior to the local current disruption, Journal of Geophysical Research: Space Physics, 114, n/a-n/a, 2009.

216 Liou, K., Meng, C.-I., Lui, A. T. Y., Newell, P. T., and Wing, S.: Magnetic dipolarization with substorm expansion onset,

217 Journal of Geophysical Research, 107, 2002.

218 Liu, W. W.: Physics of the explosive growth phase: Ballooning instability revisited, Journal of Geophysical Research: Space

219 Physics, 102, 4927-4931, 1997.

220 Liu, W. W. and Liang, J.: Disruption of magnetospheric current sheet by quasi-electrostatic field in the substorm expansion

221 phase, Annales Geophysicae, 27, 1941-1950, 2009.

222 Liu, W. W., Liang, J., and Donovan, E. F.: Electrostatic field and ion temperature drop in thin current sheets: A theory,

223 Journal of Geophysical Research: Space Physics, 115, n/a-n/a, 2010.

224 Liu, W. W., Liang, J., and Donovan, E. F.: Interaction between kinetic ballooning perturbation and thin current sheet: Quasi-

225 electrostatic field, local onset, and global characteristics, Geophysical Research Letters, 35, 2008.

226 Lui, A. T. Y., Liou, K., Nosé, M., Ohtani, S., Williams, D. J., Mukai, T., Tsuruda, K., and Kokubun, S.: Near-Earth

227 dipolarization: Evidence for a non-MHD process, Geophysical Research Letters, 26, 2905-2908, 1999.

228 Lui, A. T. Y., Lopez, R. E., Krimigis, S. M., McEntire, R. W., Zanetti, L. J., and Potemra, T. A.: A case study of magnetotail

229 current sheet disruption and diversion, Geophysical Research Letters, 15, 721-724, 1988.

230 Lui, A. T. Y., A synthesis of magnetospheric substorm models, Journal of Geophysical Research, 96,1849, 1991.

231 McFadden, J. P., Carlson, C. W., Larson, D., Ludlam, M., Abiad, R., Elliott, B., Turin, P., Marckwordt, M., and

232 Angelopoulos, V.: The THEMIS ESA Plasma Instrument and In-flight Calibration, Space Science Reviews, 141, 277-302,

233 2008.

234 Miyashita, Y., Machida, S., Mukai, T., Saito, Y., Tsuruda, K., Hayakawa, H., and Sutcliffe, P. R.: A statistical study of

235 variations in the near and middistant magnetotail associated with substorm onsets: GEOTAIL observations, Journal of

236 Geophysical Research: Space Physics, 105, 15913-15930, 2000.

237 Nagai, T.: Observed magnetic substorm signatures at synchronous altitude, Journal of Geophysical Research, 87, 4405, 1982.

238 Nakamura, R., Retino, A., Baumjohann, W., Volwerk, M., Erkaev, N., Klecker, B., Lucek, E. A., Dandouras, I., Andre, M.,

239 and Khotyaintsev, Y.: Evolution of dipolarization in the near-Earth current sheet induced by Earthward rapid flux transport,

240 Annales Geophysicae, 27, 1743-1754, 2009.

241 Nosé, M., Keika, K., Kletzing, C. A., Spence, H. E., Smith, C. W., MacDowall, R. J., Reeves, G. D., Larsen, B. A., and

242 Mitchell, D. G.: Van Allen Probes observations of magnetic field dipolarization and its associated O+ flux variations in the

243 inner magnetosphere at L < 6.6, Journal of Geophysical Research-Space Physics, 121, 7572-7589, 2016.

244 Nosé, M., Takahashi, K., Keika, K., Kistler, L. M., Koga, K., Koshiishi, H., Matsumoto, H., Shoji, M., Miyashita, Y., and

245 Nomura, R.: Magnetic fluctuations embedded in dipolarization inside geosynchronous orbit and their associated selective

246 acceleration of O+ ions, Journal of Geophysical Research: Space Physics, 119, 4639-4655, 2014.

247 Ohtani, S., Motoba, T., Gkioulidou, M., Takahashi, K., and Singer, H. J.: Spatial Development of the Dipolarization Region

248 in the Inner Magnetosphere, Journal of Geophysical Research: Space Physics, 123, 5452-5463, 2018.

249 Saito, M. H., Miyashita, Y., Fujimoto, M., Shinohara, I., Saito, Y., Liou, K., and Mukai, T.: Ballooning mode waves prior to

250 substorm-associated dipolarizations: Geotail observations, Geophysical Research Letters, 35, n/a-n/a, 2008.

251 Shiokawa, K., Baumjohann, W., Haerendel, G., Paschmann, G., Fennell, J. F., Friis-Christensen, E., Lühr, H., Reeves, G. D.,

252 Russell, C. T., Sutcliffe, P. R., and Takahashi, K.: High-speed ion flow, substorm current wedge, and multiple Pi 2

253 pulsations, Journal of Geophysical Research: Space Physics, 103, 4491-4507, 1998.

254

255

256 Figure 1 The solar wind, IMF B_z conditions and geomagnetic indices between 01:00 UT and 23:00 UT on August 27, 2014. From top to
257 bottom of (a ~ g) panels show the change of solar wind dynamic pressure (a), $B_{z,IMF}$ in GSM coordinate (b), the x component of the solar
258 wind flow speedin GSM coordinate (c), electric field E (d), *AE/AU/AL* index (e),*SYM-H* indices (f), and *ASY-H* index (g). From left to
259 right, the verticaldotted lines in (a ~ g) panels marked the time 01:48 UT, 06:42 UT, 09:31 UT, 09:48 UT, 21:56 UT and 22:35 UT,
260 respectively.

261

262 Figure 2 The orbits of TH-D and TH-E in the $X - Y_{SM}$ plane and the $X - Z_{SM}$ plane from 09:20 to 10:00 UT on 27 August 2014, which
263 were in the nightside magnetosphere. The arrow shows the flying direction of the satellites. TH-D is redand TH-E is blue.

264

265 Figure 3 The electromagnetic field and plasma parameters detected by TH-D in the intervals from 09:25 UT to 09:55 UT on August 27,
266 2014. The Solar Magnetic (SM) coordinated system is adopted. From top to bottom, panels showed that (a)the total magnetic field B_t
267 (black) and the X component B_x (red), (b) the Y component B_y (green) and the Z component B_z (blue), (c)the magnetic field elevation
268 angle θ; (d) ion and electron density N_i, N_e; (e)ion and electron temperature T_i, T_e; (f) plasma beta β; (g) the X component of ion
269 parallelvelocity and perpendicular velocity V_{parx}, V_{perpx}; (h) the Y component of ion parallel velocity and perpendicularvelocity
270 V_{pary},V_{perpy}; (i) the Z component of ion parallel velocity and perpendicular velocity V_{parz}, V_{perpz} ; (j) the electric field E_x (red), E_y
271 (black), and E_z (blue) by assuming $\mathbf{E} \cdot \mathbf{B} = \mathbf{0}$; (k) the electric field E_{cx} (red), E_{cy} (black), E_{cz} (blue) calculated by $\mathbf{E} = \mathbf{B} \times \mathbf{V}$. The black
272 vertical dashed lines marked the time 09:30:34 UT, 09:30:54 UT, 09:36:06 UT and 09:36:21 UT, respectively.
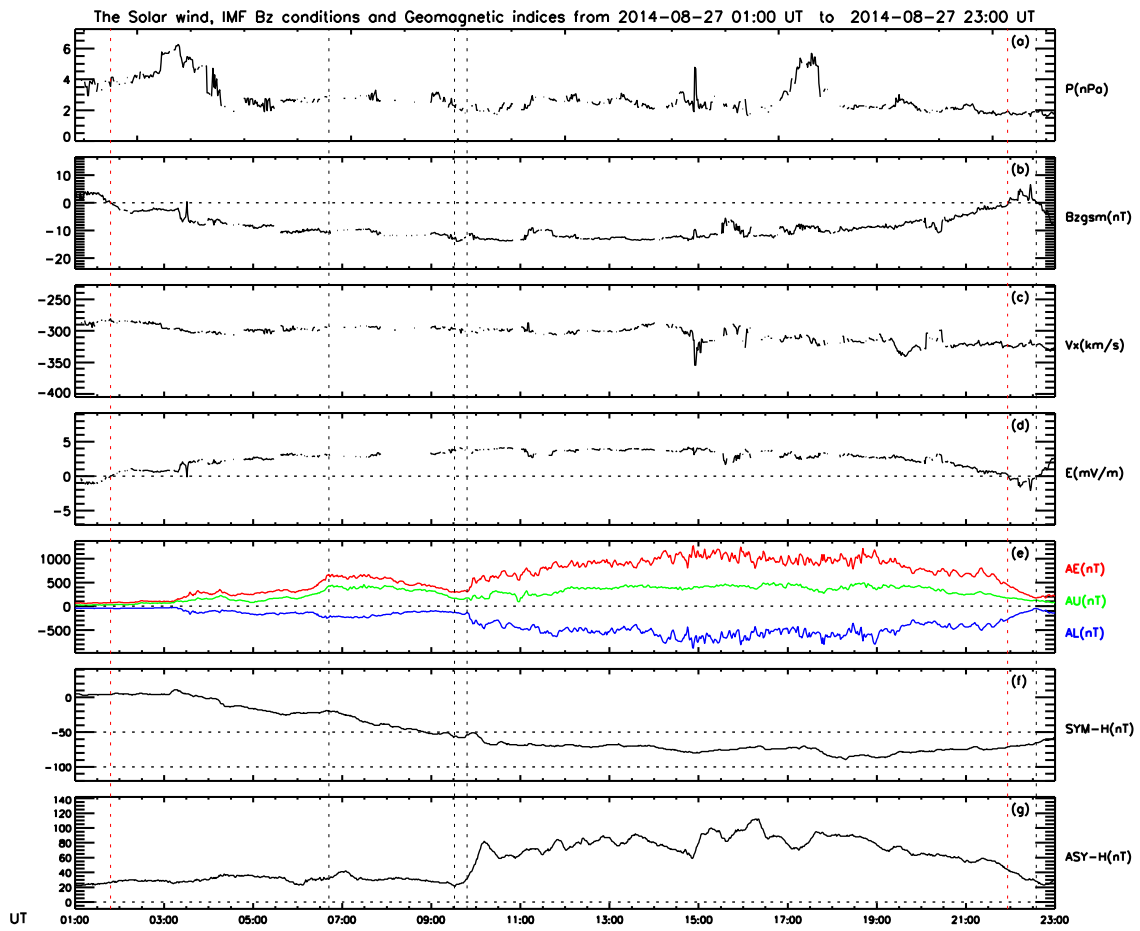
273

274 Figure 4 The electromagnetic field and plasma parameters detected by TH-E in the intervals from 09:25 UT to 09:55 UT on August 27,
275 2014.The Figure format is the same as Figure 3.The black vertical dashed lines marked the time 09:35:36 UT and 09:36:18 UT.
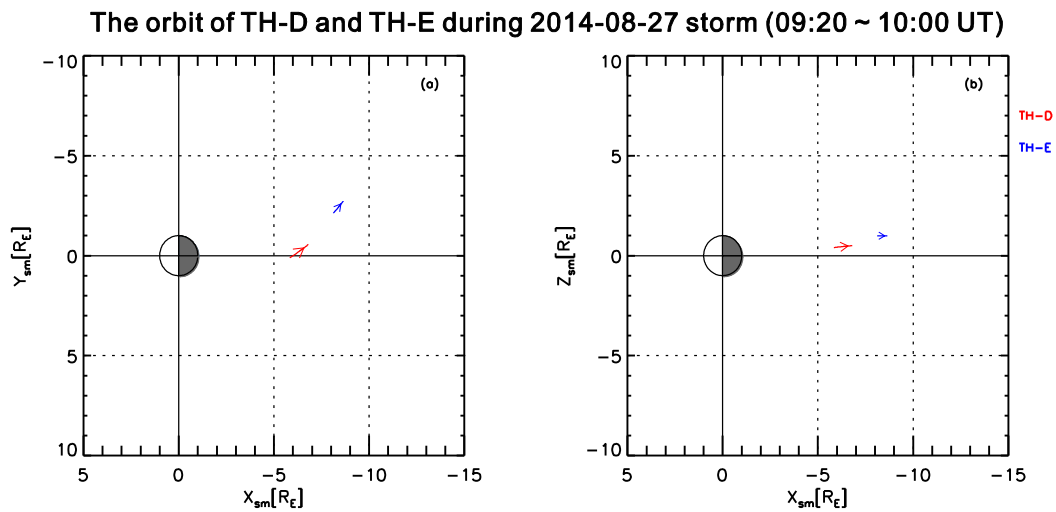
276

277 Figure 5 The energy flux and pitch angle distribution of energetic electrons detected by SST/TH-D in 3 second time resolution. The red
278 vertical lines marked the time 09:30:38 UT and 09:36:09 UT.
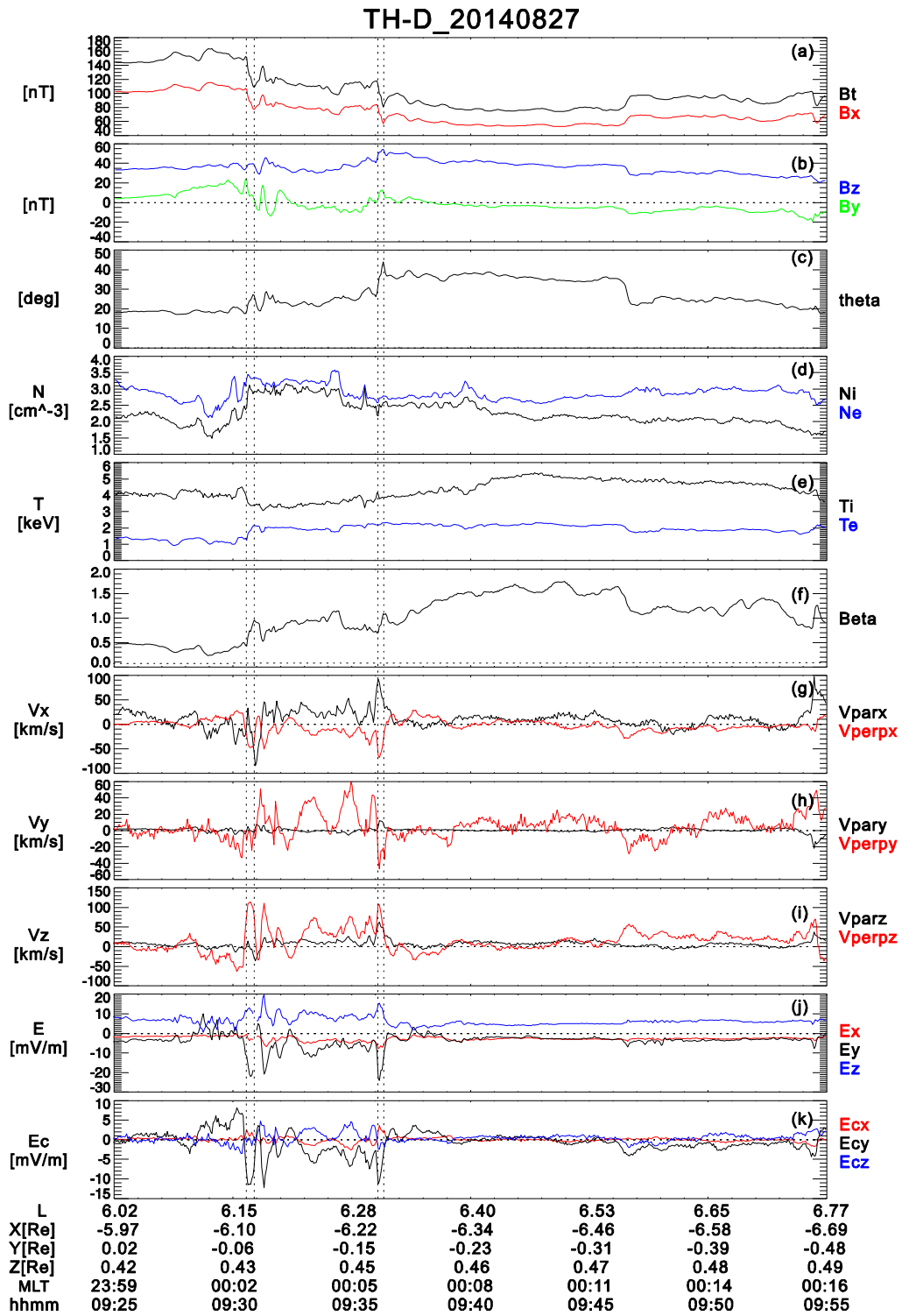
279

10

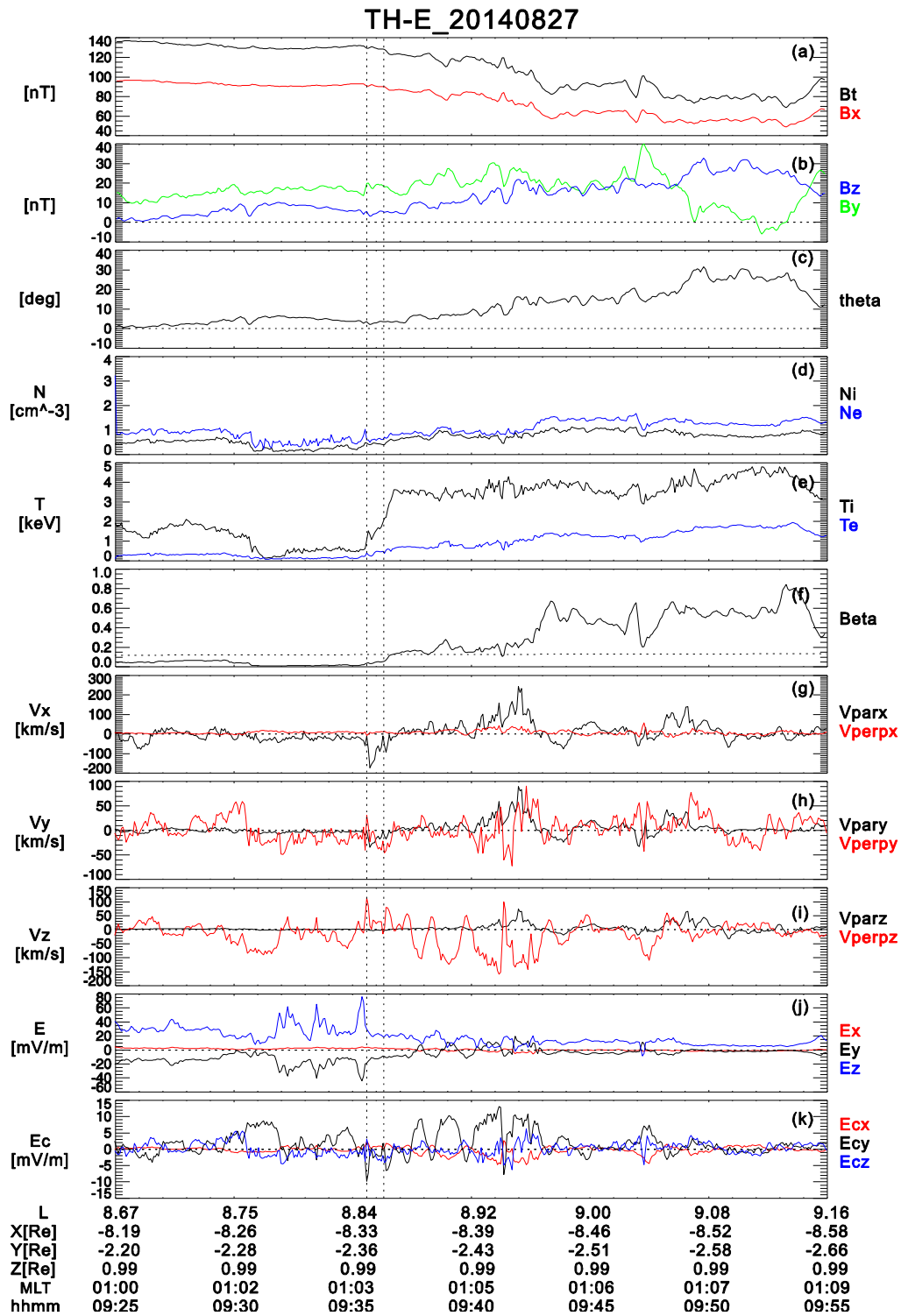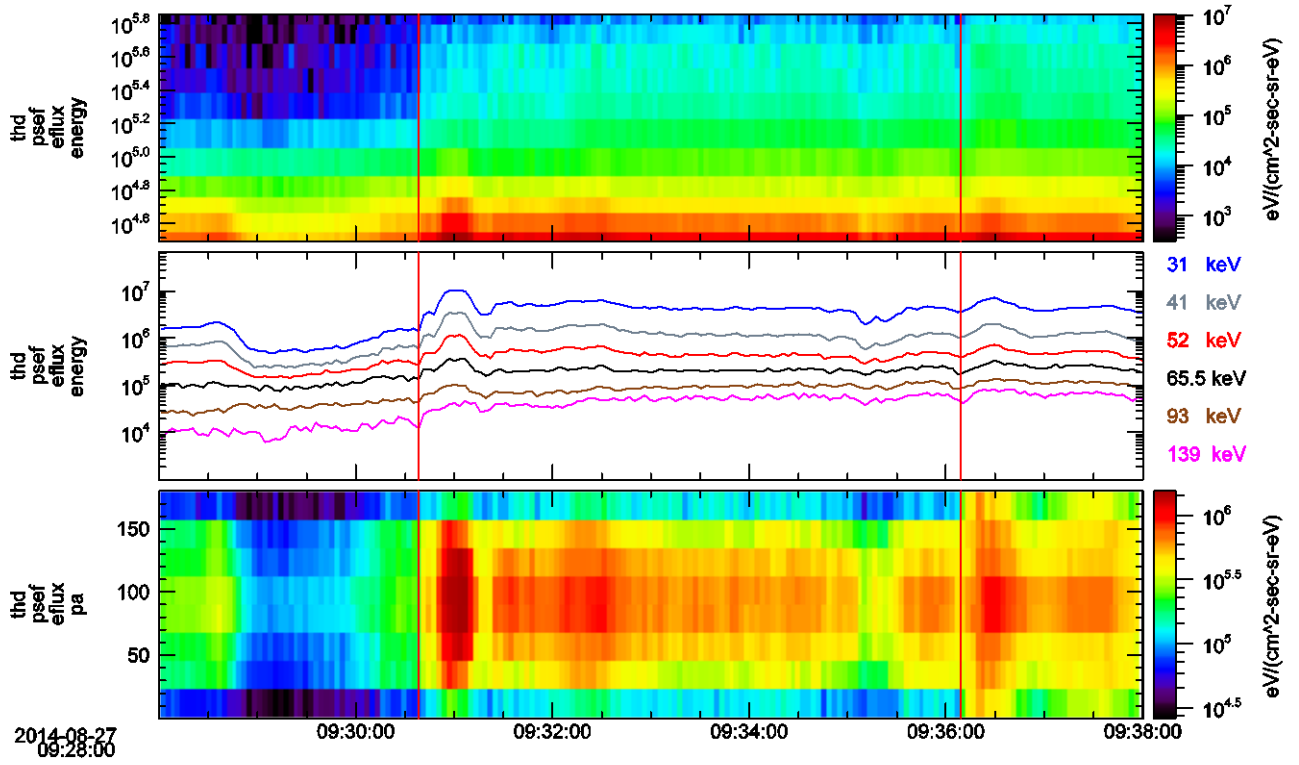280   Figure 1

The Solar wind, IMF Bz conditions and Geomagnetic indices from 2014-08-27 01:00 UT to 2014-08-27 23:00 UT

281

282   Figure 2

The orbit of TH-D and TH-E during 2014-08-27 storm (09:20 ~ 10:00 UT)

283

TH-D_20140827

TH-E_20140827

L	8.67	8.75	8.84	8.92	9.00	9.08	9.16
X[Re]	-8.19	-8.26	-8.33	-8.39	-8.46	-8.52	-8.58
Y[Re]	-2.20	-2.28	-2.36	-2.43	-2.51	-2.58	-2.66
Z[Re]	0.99	0.99	0.99	0.99	0.99	0.99	0.99
MLT	01:00	01:02	01:03	01:05	01:06	01:07	01:09
hhmm	09:25	09:30	09:35	09:40	09:45	09:50	09:55

287

288   Figure 5

289
290